Adsorption 11: 737–743, 2005


# Comparison of Adsorption Properties of Polymer-Templated Mesoporous Silicas with Incorporated Niobium

IZABELA NOWAK*
*Adam Mickiewicz University, Faculty of Chemistry, Grunwaldzka 6, PL-60-780 Poznan, Poland*
nowakiza@amu.edu.pl

MIETEK JARONIEC
*Kent State University, Department of Chemistry, Kent, Ohio 44240, USA*
jaroniec@kent.edu

MARIA ZIOLEK
*Adam Mickiewicz University, Faculty of Chemistry, Grunwaldzka 6, PL-60-780 Poznan, Poland*

**Abstract.** Two types of Nb-containing mesoporous materials were studied: (i) NbSBA-15 with 2D-hexagonal structure and (ii) NbFDU-1 with cage-like structure. The elucidation of the pore connectivity and the pore blockage on the basis of nitrogen and argon desorption isotherms combined with FTIR and $H_2$-TPR studies is presented for niobium-containing materials. Moreover, the surface properties are studied by FTIR with NO, while the catalytic activity is examined by sulfide and cyclohexene oxidation with hydrogen peroxide.

**Keywords:** adsorption, catalysis, niobium, polymer-templating synthesis

## 1. Introduction

Niobium belongs to the transition metals that isomorphously substitute silicon in the structures of ordered mesoporous materials (OMMs) first reported in 1992 (Kresge et al.). In the past few years much work has been done on the surfactant-templated material, NbMCM-41, and several synthesis routes have been developed for this material (Ziolek and Nowak, 1997; Zhang and Ying, 1997; Nowak, 2002, 2004; Hartmann et al., 2003; Parvulescu et al., 2003). There has been a growing interest in the synthesis of other OMMs containing niobium, especially polymer-templated ones, which are attractive for adsorption, catalysis and immobilization of molecules. The polymeric templates provide great opportunities for the pore size and pore structure engineering.

*To whom correspondence should be addressed.

In this work two kinds of triblock copolymers of ABA type were chosen to synthesize two different structures: SBA-15, which is the 2D hexagonal array of ordered mesopores interconnected by irregular micropores, and FDU-1, which is a cage-like mesoporous structure with complementary microporosity. So far, the adsorption properties of NbSBA-15 and NbFDU-1 materials have been investigated by nitrogen adsorption. This study is focused on the argon adsorption analysis of polymer-templated mesoporous molecular sieves prepared with different triblock-copolymers of similar EO/PO and EO/BO ratios, where EO, PO and BO denote ethylene, propylene and butylene oxides. It is known that argon at 77 K is suitable for studying porosity of materials with pores below 15 nm (Kruk et al., 2003). Here, low-temperature (77 K) argon adsorption data will be used for characterization of ordered siliceous mesostructures containing niobium and for assessment of their quality.

The incorporation of niobium was monitored by chemical analysis and hydrogen temperature-programmed reduction ($H_2$-TPR). The textural/structural/surface properties were investigated by X-ray diffraction (XRD) and Infrared Spectroscopy combined with NO (FTIR/NO). Moreover, the catalytic activity was examined by phenyl methyl sulfide and cyclohexene oxidation with hydrogen peroxide.

## 2. Synthesis

Niobosilicate samples of NbSBA-15 and NbFDU-1 were synthesized as reported elsewhere (Nowak et al., 2004, Nowak and Jaroniec, 2005). Both materials were prepared using tetraethyl orthosilicate - TEOS (Aldrich) and niobium(V) oxalate (CBMM, Brazil) as silicon and niobium sources, respectively. The Si/Nb atomic ratio was kept 64. Two different triblock-copolymers were used, i.e., BASF Pluronic P103—$(EO)_{38}(PO)_{56}(EO)_{38}$ and Dow Chemicals B50-6600—$(EO)_{39}(BO)_{47}(EO)_{39}$, for the synthesis of NbSBA-15 and NbFDU-1, respectively, to investigate the effect of the polymer structure on the porosity of the resulting material. The hydrothermal treatment was carried out at 353 K for 16 h for NbSBA-15 and 373 K for 6 h for NbFDU-1 in order to obtain a similar contribution of micropores fraction (around one third of the total pore volume). The precipitate in both cases was filtered, dried and calcined at 823 K for 8 h.

## 3. Characterization

### 3.1. Nitrogen and Argon Low-Temperature Adsorption

The physical adsorption/desorption isotherms of nitrogen and argon were recorded on a Micromeritics 2010 instrument. For these measurements about 200 mg of each sample was degassed under vacuum at 473 K for 2 h. The BET surface area was calculated from the data acquired in the relative pressure ($p/p_0$) range of 0.05 to 0.2. The cross-sectional areas of 0.162 and 0.138 $nm^2$ were used for nitrogen molecule and argon atom, respectively, in the BET calculations. The volumes of micropores, $V_{mi}$, and mesopores, $V_p$, were assessed using the $\alpha_s$ plot method (Jaroniec et al., 1999), where $\alpha_s$ is the standard relative adsorption defined as the amount adsorbed on a reference adsorbent (in this case LiChrospher Si-1000) at a given relative pressure divided by the amount adsorbed at the relative pressure of 0.4. The micropore volume was calculated in the $\alpha_s$ range from 0.9 to 1.2, i.e., from the linear segment of the $\alpha_s$ plot below the onset of capillary condensation. The volume of primary mesopores was evaluated in the range of $\alpha_s$ from 1.8 to 2.2, i.e., from a linear segment of the $\alpha_s$ plot that appears after completion of the capillary condensation step. The pore size distribution (PSD) was calculated from the adsorption branch of isotherms by using the Barrett-Joyner-Halenda (BJH) method modified by Kruk et al. (1997) known as the KJS method. The diameter of primary mesopores, $w_{PSD}$, is defined as the maximum on PSD. Moreover, due to the fact that the geometry of primary mesopores of FDU-1 can be approximated by a sphere rather than a cylinder, this method leads to a systematic underestimation of the size of cage-like pores by about 2 nm (Matos et al., 2003). Thus, the primary mesopore cage diameter of FDU-1, $w^*$, was estimated on the basis of the unit-cell size assessed from XRD and the pore volumes assessed from gas adsorption data, i.e., $V_p$ and $V_{mi}$ from the $\alpha_s$ plot according to the following formula (Matos et al., 2003):

$$w^* = 0.78 \cdot a_0 \cdot \left( \frac{V_p}{1/\rho + V_{mi} + V_p} \right)^{1/3} \quad (1)$$

where $\rho$ is the silica density equal to 2.2 g $cm^{-3}$. For SBA-15 the following formulae was used (Kruk et al., 2003):

$$w^* = 1.05 \cdot a_0 \cdot \left( \frac{V_p}{1/\rho + V_{mi} + V_p} \right)^{1/2} \quad (2)$$

### 3.2. X-Ray Diffraction (XRD)

XRD measurements were made on TUR-62 using Ni-filtered Cu $K_\alpha$ radiation (0.15418 nm). The XRD data were collected in the $2\theta$-region of 1.4 to 10° at a step size 0.02°. The data were also collected in the $2\theta$-region of 10–60° to monitor the formation of bulk niobium oxide, if any.

### 3.3. $H_2$-TPR

Temperature-programmed reduction (TPR) was conducted using a conventional apparatus (Micromeritics PulseChemisorb 2705) equipped with a thermal conductivity detector. Each sample was pre-treated in a

helium flow at 673 K for 1 h, and cooled down to room temperature (RT). The reduction was performed by heating the sample from 298 up to 1373 K at a rate of 10 K $min^{-1}$ using a 10 vol% $H_2$/Ar mixture flow (32 $cm^3$ $min^{-1}$).

### 3.4. FTIR Spectroscopy

IR spectra were recorded in absorbance mode using a vacuum cell, prior to and after dosing nitrogen (II) oxide - NO at room temperature. A self-supported sample wafer weighing 10 mg $cm^{-2}$ was activated by heating in situ for 3 h at a temperature of 723 K and under a vacuum of $10^{-3}$ Torr prior to its exposure to NO. A Bruker Vector 22 FTIR spectrometer was employed and 128 scans were collected at a resolution of 2 $cm^{-1}$ for recording each spectrum. The IR spectra of the activated samples were subtracted from those registered after NO adsorption at RT followed by various treatments. The reported spectra reflect data after this subtraction. Only the spectra shown in the 850–1000 $cm^{-1}$ region are original without subtraction of the spectrum after activation.

### 3.5. Catalytic Oxidation

In a typical oxidation run, 0.04 g of the catalyst and 10 $cm^3$ of acetonitrile as solvent were fed in the batch reactor and the mixture was heated up to 318 and 323 K for cyclohexene and phenyl methyl sulfide, respectively, under vigorous stirring. At that temperature, 2 mmol of substrate followed by 2 mmol of hydrogen peroxide (∼34 wt% aqueous solution) were added. The reaction time was 40 and 12 h for cyclohexene and phenyl methyl sulfide, respectively. Samples of the cyclohexene oxidation were taken after each 40 min and analyzed using a Carlo Erba GC8000 Top gas chromatograph equipped with a DB-1 capillary column and a flame ionization detector (FID). The organic phase of sulfide oxidation was analyzed by gas chromatography (SRI 8610 chromatograph) using an on-line capillary column (Porapak QS) and FID detector. The identification of the products in both cases was achieved from the retention time of the pure compounds and occasionally by GC-MS.

## 4. Results and Discussion

The actual Si/Nb ratio in the calcined samples was determined by EDX (Shimadzu EDX 700) to be 165 for NbFDU-1 and 141 for NbSBA-15. The use of the acidic synthesis conditions for the preparation of Nb-containing materials led to about twice lower amount of niobium incorporated.

The XRD patterns are characteristic of mesoporous materials of SBA-15 and FDU-1 materials with typical $d_{100}$ (strong), $d_{110}$ and $d_{200}$ (weak) for NbSBA15, and $d_{111}$ (strong) and several other (weak) reflections for NbFDU-1. No obvious differences could be observed from the XRD patterns (not shown here) for these two niobium-containing samples and pure silica ones, suggesting that the characteristic mesoporous structure is well preserved after introducing Nb into the skeleton. These samples could be indexed on the basis of a hexagonal unit cell with $a_0 = 10.6$ nm and of a cubic cell with $a_0 = 21.9$ nm, for NbSBA-15 and NbFDU-1, respectively (see Table 1).

It is known (Ziolek et al., 2001) that the low temperature (*LT*) peaks (below ∼1000 K) are due to the reduction of extra-framework niobium species, whereas, those at high temperatures (HT) - above ∼1000 K—characterize the reduction of niobium localized in the framework of MCM-41 samples. The reduction profiles of NbSBA-15 and NbFDU-1 samples are shown in Fig. 1. Two of the TPR peaks for NbFDU-1, at ∼900 and 1350 K, are like those observed for the niobosiliceous MCM-41 material (2D hexagonal mesostructure) and were assigned to the extra-framework and framework niobium species,

*Table 1.* Textural/structural properties of Nb-containing samples.

| | | BET($m^2g^{-1}$) | | $w_{PSD}$ (nm) | | $V_p$ ($cm^3g^{-1}$) | | $V_{mi}$ ($cm^3g^{-1}$) | | |
|---|---|---|---|---|---|---|---|---|---|---|
| Sample | $a_0$ (nm) | $N_2$ | Ar | $N_2$ | Ar | $N_2$ | Ar | $N_2$ | Ar | $w^*$ (nm) |
| NbSBA-15 | 10.6 | 780 | 700 | 7.4 | 7.6 | 0.38 | 0.39 | 0.18 (33%) | 0.11 (23%) | 7.4 |
| NbFDU-1 | 21.7 | 970 | 850 | 11.2 | 10.1 | 0.48 | 0.56 | 0.29 (38%) | 0.21 (27%) | 12.5 |

*Calculated from Eqs. (1) and (2).

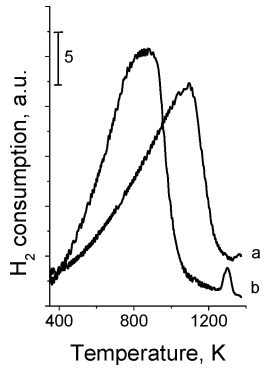


*Figure 1.* $H_2$-TPR profiles of NbSBA-15 (a) and NbFDU-1 (b).

respectively. For NbSBA-15 material such peaks are shifted into the higher temperature suggesting that the reduction of niobium species is more difficult. Besides being less intense, the shape of the reduction peak at 1050 K for NbSBA-15 is considerably different from that observed for the NbFDU-1 sample. The broad low-temperature peak suggests increasing hydrogen consumption by more than one reduced species. The above stated features can suggest that extra-framework niobium covers framework niobium species in the case of NbSBA-15. A more evident presence of framework niobium is in the case of the NbFDU-1 sample. In this material more than one niobium species was also detected.

The incorporation of niobium into the silica framework, at the concentrations used here, produces small particles of extra-framework niobium oxide species, typically $Nb_2O_5$. The presence of $Nb_2O_5$ particles in the two different samples was also supported by the FTIR and wide-angle XRD results (not shown), which is evidenced by the characteristic $Nb_2O_5$ band at about 680 $cm^{-1}$ and reflections at $2\theta = 22.5^\circ$, $28.3^\circ$ typical for orthorhombic crystalline $Nb_2O_5$. The presence of extra-framework niobium in the form of crystalline niobium oxide causes the pore or cavity entrance blockage that will be further studied by nitrogen and argon adsorption/desorption.

Nitrogen and argon adsorption isotherms (type IV) at 77 K (Fig. 2) confirm that both samples possess well-defined mesoporosity. Adsorption parameters for the materials synthesized in this project are summarized in Table 1. The Nb-containing materials have the BET specific surface of about 800–1000 $m^2\,g^{-1}$ and the mesopore volume of about 0.5 $cm^3\,g^{-1}$ similar to those observed for siliceous FDU-1 and SBA-15. The BET surface areas and pore volumes for NbSBA-15 and NbFDU-1 were also measured with argon adsorption and the results are included in Table 1. There is a good consistency between argon and nitrogen adsorption measurements.

The initial portion of the isotherm corresponds to the adsorption in micropores and formation of a multilayer film on the pore walls. NbFDU-1 and NbSBA-15 contain intrawall micropores (their amount is shown in Table 1) that are typical for the materials prepared using polymeric surfactants with EO blocks. As expected for SBA-15 silicas, the NbSBA-15 sample is appreciably microporous (~33 and 23% of the total porosity are micropores from nitrogen and argon adsorption,

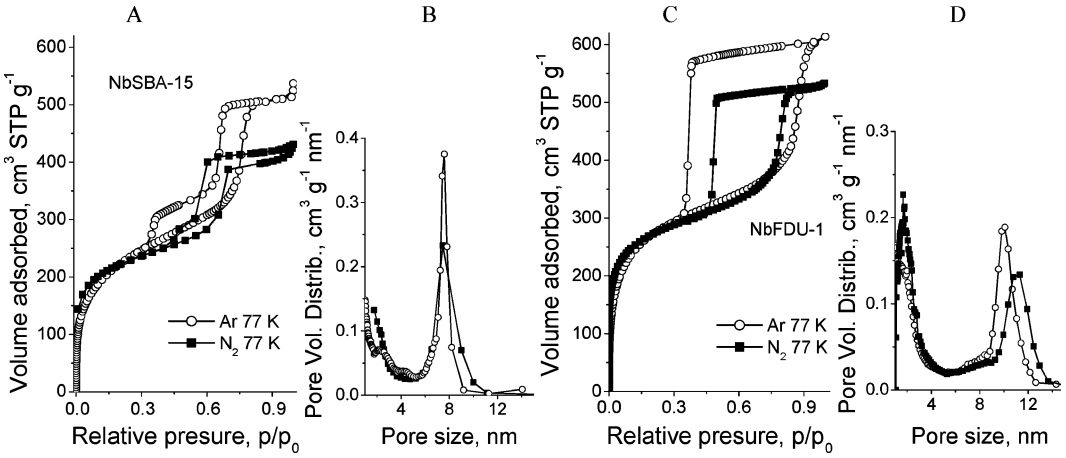


*Figure 2.* Nitrogen and argon adsorption isotherms at 77 K (A,C) and pore size distributions (B,D) for the NbSBA-15 (A,B) and NbFDU-1 (C,D) materials.

respectively), while NbFDU-1 shows slightly higher amount of micropores (∼38 and 27%), however the low-size PSD of the latter sample is shifted to higher values (Fig. 2(B) and (D)). The mesopore diameter is about ∼7.4 and ∼11.2 nm for NbSBA-15 and NbFDU-1, respectively.

Adsorption isotherms for NbSBA-15 are shown in Fig. 2(A). They exhibit sharp steps in the relative pressure of about 0.65 for nitrogen and 0.7 for argon, respectively, which reflect the capillary condensation in the channels of SBA-15. It can be seen that for argon adsorption, this steep is more vertical and shifted to higher relative pressures. Moreover, the hysteresis loop for $N_2$ isotherm (type H1) is slightly broader and exhibits some tailing that can be arise from constrictions in the porous structure. Argon adsorption hysteresis is closed quite abruptly in the proximity of the lower limit of adsorption/desorption hysteresis, which indicates that these constrictions are below 4 nm. The influence of the extra-framework niobium formation ($H_2$-TPR and FTIR/XRD studies) on the porous system is thus confirmed.

By employing argon adsorption the cavity entrance size of NbFDU-1 can be established. It was shown (Kruk and Jaroniec, 2003; Matos et al., 2003) that a bigger difference between nitrogen and argon adsorption curves in the area of condensation step is connected with a larger entrance. Moreover, for the cavity entrance sizes in the range from 1.3 to 4 nm there was steep decline of the desorption branches of nitrogen and argon isotherms above the lower limit of hysteresis, for entrances above 4 and below 5 nm—a gradual decline was observed for the argon desorption branch, while for entrances above 5 nm—a gradual decline of nitrogen and argon desorption branches was visible. Thus, in our case the entrance size was estimated to be ∼3 nm (Fig. 2(C)). It seems that the cavitation effect is observed here, not a pore blocking, due to a big difference between the cavity size and entrance.

To examine the niobium location in mesoporous molecular sieves the FTIR spectroscopy using a standard self-supporting pellet was employed. It is well-known (Broclawik et al., 2000; Sponer et al., 2001) that upon coordination of metal cations to the framework oxygens of high silica zeolites new, intense bands appear in the transmission window between the antisymmetric (∼1100 $cm^{-1}$) and symmetric (800 $cm^{-1}$) T-O-T stretching modes. The new bands have been ascribed to the T-O-T skeletal stretching modes, shifted (red shift) due to a perturbation caused by cation coordination (referred to as the "deformation shift"). Moreover, the coordination of electron donor ligands such as NO to the metal cations changes the strength of the bond between the metal and the framework oxygens and hence it is detectable in the infrared spectra (a blue shift of about 10–20 $cm^{-1}$). Both niobium-containing samples studied show a few IR bands suggesting the presence of various niobium species. In both cases a high shift of the perturbed T-O-T band to the lower wavenumbers (1000–950 $cm^{-1}$) is visible (Fig. 3). It indicates the excessive influence of Nb-species on the T-O-T vibration. For NbSBA-15 after adsorption of NO almost no shift in the infrared spectra was observed while a small one for NbFDU-1 material (compare Fig. 3(A) and (B)). The band at 960 $cm^{-1}$ for NbFDU-1 is shifted by 10 $cm^{-1}$ that indicates very high "relaxation shift"

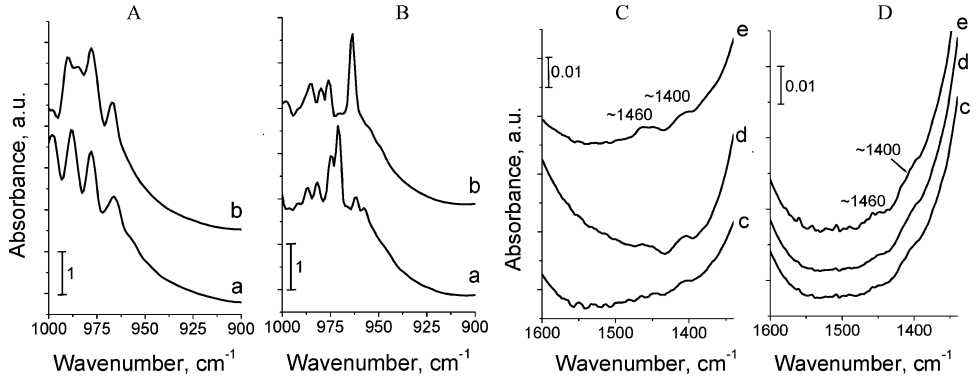


*Figure 3.* FTIR spectra for NbSBA-15 (A,C) and NbFDU-1 (B,D) recorded in the vacuum IR cell without subtraction (A,B): (a) after evacuation at 723 K, 3 h; (b) after NO adsorption at RT; and after subtraction of the spectrum after activation (C,D): (c) after NO adsorption at RT, 3 h; followed by the evacuation at: (d) RT, 0.5 h, and (e) 373 K, 0.5 h.

*Table 2*. Catalytic behaviors of NbSBA-15 and NbFDU-1 towards oxidations of cyclohexene and phenyl methyl sulfide with hydrogen peroxide at 318 and 323 K, respectively.

| | | Selectivity (%)[a] | | | Selectivity (%)[b] | |
|---|---|---|---|---|---|---|
| Catalysts | $C_6H_{10}$ conversion (%)[a] | $C_6H_{10}O$ | $C_6H_{10}(OH)_2$ | $PhSCH_3$ conversion (%)[b] | $PhSOCH_3$ | $PhSO_2CH_3$ |
| NbSBA-15 | 29 | 20 | 75 | 15 | 55 | 45 |
| NbFDU-1 | 10 | 30 | 70 | 9 | 63 | 37 |

[a] After 40 h.
[b] After 12 h.

suggesting strong bonding of NO with niobium species in the case of NbFDU-1. Such a phenomenon can suggest easy access to the niobium localized in the framework, thus no blocking effect exists in this material. Therefore, we believe that extra-framework niobium species are located outside the cavities of NbFDU-1. The presence of framework niobium for NbSBA-15 (i.e., the occurrence of the "relaxation shift") is not so clear in agreement with $H_2$-TPR results.

The surface properties of the above mentioned samples were studied by NO interaction with the niobium-species by analysis of the FTIR spectra in the 1300–2200 $cm^{-1}$ region. Fig. 3(C) and (D) show that the adsorption of NO at RT on both samples leads to the formation of nitrato/nitrito species at the wavenumbers below 1600 $cm^{-1}$. The results presented in Fig. 3(C) and (D) indicate the oxidizing properties of both materials.

Mesoporous host materials with one dimensional (SBA-15) and three-dimensional (FDU-1) channel systems were compared in the oxidation processes. The two different host systems were chosen because of their suggested differences in catalytic applications due to the pore blocking effects, which are much more likely for NbSBA-15 or due to small cavity entrance—for NbFDU-1. The catalytic activity and selectivity in the oxidation of cyclohexene and phenyl methyl sulfide over NbSBA-15 and NbFDU-1 are shown in Table 2.

Cyclohexene is oxidized to produce cyclohexene diol as a main product together with cyclohexene oxide as by-product. The major product in phenyl methyl sulfide oxidation is sulfoxide, a desired product regarding its biological and pharmacological properties. The results given in Table 2 show that, in the case of both oxidation reactions, NbSBA-15 catalyst is more active than NbFDU-1. It may be a consequence of the easier diffusion of the sulfide through the pores of SBA-15 (7 nm channel) than in the cavities of NbFDU-1 (∼11 nm cavity with ∼3 nm entrance). Interestingly, for alkene oxidation the structure factor is especially influencing the conversion, while it is less pronounced for sulfide. NbSBA-15 material is effective for both reactions studied; however activities and yields of desired products are lower than those for NbMCM-41 materials. This fact can be explained by more effective isolation of niobium species in the MCM-41 matrix (Nowak and Ziolek, 2005).

## 5. Conclusions

The NbSBA-15 and NbFDU-1 materials prepared by niobium incorporation during the synthesis in acidic aqueous media have a hexagonally ordered structure of uniform mesopores with some pore constrictions less than 4 nm and a cage-like structure with cavities of 11 nm and entrance sizes of ∼3 nm, respectively. Niobium is believed to be located partially in the framework positions in both cases; however the presence of extra-framework niobium was also established. In NbFDU-1 extra-framework species are situated outside the cavities, whereas in NbSBA-15 they are placed in the channels. Both niobium-containing mesoporous molecular sieves exhibit oxidative properties as revealed by NO/FTIR studies and consequently, show catalytic activity in oxidation processes.

## Acknowledgment

I.N. and M.Z. acknowledge a financial support by the Polish State Committee for Scientific Research (grant no. 3T09A 100 26; 2004–2007). M.J. acknowledges support by NSF Grant CHE-0093707. The authors thank BASF and Dow Chemicals for providing triblock copolymers and CBMM (Brazil) – for niobium (V) oxalate.

## References


Broclawik, E., J. Datka, B. Gil, and P. Kozyra, "T-O-T Skeletal Vibration in CuZSM-5 Zeolite: IR Study and Quantum Chemical Modeling," *Phys. Chem. Chem. Phys.*, **2**, 401–405 (2000).

Hartmann, M., A.M. Prakash, and L. Kevan, "Characterization and Catalytic Evaluation of Mesoporous and Microporous Molecular Sieves Containing Niobium," *Catal. Today*, **78**, 467–475 (2003).

Jaroniec, M., M. Kruk, and J.P. Olivier, "Standard Nitrogen Adsorption Data For Characterization of Nanoporous Silicas," *Langmuir*, **15**, 5410–5413 (1999).

Kresge, C.T., M.E. Leonowicz, W.J. Roth, J.C. Vartuli, and J.S. Beck, "Ordered Mesoporous Molecular-Sieves Synthesized by a Liquid-Crystal Template Mechanism," *Nature*, **359**, 710–712 (1992).

Kruk, M. and M. Jaroniec, "Argon Adsorption at 77 K as a Useful Tool for the Elucidation of Pore Connectivity in Ordered Materials With Large Cagelike Mesopores," *Chem. Mater*., **15**, 2942–2949 (2003).

Kruk, M., M. Jaroniec, and A. Sayari, "Application of Large Pore MCM-41 Molecular Sieves to Improve Pore Size Analysis Using Nitrogen Adsorption Measurements," *Langmuir*, **13**, 6267–6273 (1997).

Kruk, M., M. Jaroniec, S.H. Joo, and R. Ryoo, "Characterization of Regular and Plugged SBA-15 Silicas by Using Adsorption and Inverse Carbon Replication and Explanation of the Plug Formation Mechanism," *J. Phys. Chem. B*, **107**, 2205–2213 (2003).

Matos, J.R., M. Kruk, L.P. Mercuri, M. Jaroniec, L. Zhao, T. Kamiyama, O. Terasaki, T.J. Pinnavaia, and Y. Liu, "Ordered Mesoporous Silica With Large Cage-Like Pores," *J. Am. Chem. Soc.*, **125**, 821–829 (2003).

Nowak, I., "The Effect of Niobium Source Used in the Synthesis on The Properties of NbMCM-41 Materials," *Stud. Surf. Sci. Catal.*, **142**, 1363–1370 (2002).

Nowak, I., "Textural and Structural Properties of Niobium-Containing Micro-, Meso- and Macroporous Molecular Sieves," *Coll. Surf. A: Physicochem. & Eng. Aspects*, **241**, 103–111 (2004).

Nowak, I. and M. Jaroniec, "Three-Dimensional Cubic Mesoporous Molecular Sieves of FDU-1 Containing Niobium: Dependence of Niobium Source on Surface Properties," *Langmuir*, **21**, 755–760 (2005).

Nowak, I. and M. Ziolek, "Effect of Texture and Structure on The Catalytic Activity of Mesoporous Niobosilicates for the Oxidation of Cyclohexene," *Microporous Mesoporous Mater.*, **78**, 281–288 (2005).

Nowak, I., M. Ziolek, and M. Jaroniec, "Synthesis and Characterization of Polymer-Templated Mesoporous Silicas Containing Niobium," *J. Phys. Chem. B*, **108**, 3722–3727 (2004).

Parvulescu, V., C. Anastasescu, C. Constantin, and B.L. Su, "Mono (V, Nb) or Bimetallic (V-Ti, Nb-Ti) Ions Modified MCM-41 Catalysts: Synthesis, Characterization and Catalysis in Oxidation of Hydrocarbons (Aromatics and Alcohols)," *Catal. Today*, **78**, 477–485 (2003).

Sponer, J.E., Z. Sobalik, J. Leszczynski, and B. Wichterlova," Effect of Metal Coordination on the Charge Distribution Over The Cation Binding Sites of Zeolites," *J. Phys. Chem. B*, **105**, 8285–8290 (2001).

Zhang, L. and J.Y. Ying, "Synthesis and Characterization of Mesoporous Niobium-Doped Silica Molecular Sieves," *AIChE J.*, **43**, 2793–2801 (1997).

Ziolek, M. and I. Nowak, "Synthesis and Characterization of Niobium-Containing MCM-41," *Zeolites*, **18**, 356–360 (1997).

Ziolek, M., I. Sobczak, A. Lewandowska, I. Nowak, P. Decyk, M. Renn, and B. Jankowska, "Oxidative Properties of Niobium-Containing Mesoporous Silica Catalysts," *Catal. Today*, **70**, 169–181 (2001).